Observation of the fcc-to-hcp Transition in Ensembles of Argon Nanoclusters

N. V. Krainyukova, R. E. Boltnev, E. P. Bernard, V. V. Khmelenko, D. M. Lee, and V. Kiryukhin

Phys. Rev. Lett. **109**, 245505 — Published 13 December 2012

DOI: 10.1103/PhysRevLett.109.245505

Observation of the fcc-to-hcp transition in ensembles of argon nanoclusters

N.V. Krainyukova[1], R.E. Boltnev[2], E.P. Bernard[3†], V.V. Khmelenko[4], D.M. Lee[4], and V. Kiryukhin[5*]

1. B. Verkin Institute for Low Temperature Physics and Engineering of the National Academy of Sciences of Ukraine, 47 Lenin Ave., Kharkov, Ukraine

2. Branch of Institute of Energy Problems of Chemical Physics, Chernogolovka, Moscow Region, 142432, Russia

3. Laboratory of Atomic and Solid State Physics, Cornell University, Ithaca, New York 14853, USA

4. Department of Physics and Astronomy, Texas A&M University, College Station, Texas 77845, USA

5. Department of Physics and Astronomy, Rutgers University, Piscataway, New Jersey 08854, USA

† Present address: Department of Physics, Yale University, New Haven, Connecticut 06511, USA

*email: vkir@physics.rutgers.edu

Abstract

Macroscopic ensembles of weakly-interacting argon nanoclusters are studied using x-ray diffraction in low vacuum. As the clusters grow by fusion with increasing temperature, their structure transforms from essentially face-centered cubic (fcc) to hexagonal close packed (hcp) as the cluster size approaches ~10^5 atoms. The transformation involves intermediate orthorhombic phases. These data confirm extant theoretical predictions. They also indicate that growth kinetics and spatial constraints might play an important role in the formation of the fcc structure of bulk rare-gas solids, which still remains puzzling.

Understanding structural transitions and predicting crystal structure are among the key tasks of condensed matter physics and materials science. Rare-gas solids (RGS) consist of weakly-interacting, nearly-spherical atoms with fully filled electronic shells. They crystallize in close-packed structures, and are chemically inert insulators at ambient pressures. Uncovering the physics of these simple materials is a necessary step towards understanding more complex phases of matter. Classical (neon and heavier) RGS crystallize in the face-centered cubic (fcc) structure at ambient pressure. Early theories, however, predicted the hexagonal close packed (hcp) structure, giving rise to the well-known "RGS structure problem".[1,2] The fcc and hcp structures differ by their stacking patterns of the close-packed triangular layers: ABC for the fcc, and ABAB for the hcp (A, B, and C refer to the three possible positions of the layers on top of each other). The difficulty of the RGS structure problem stems from the minute energy differences between these structures (about 0.01% of the binding energy)[1]. In rare gas solids, weak van der Waals interatomic interactions dominate. This presents a difficulty for various ab-initio calculations, such as density functional theory.[3-6] Calculations based on two- and many-body interaction potentials, including those accounting for zero-point contributions, have been therefore widely utilized to describe the rare gas solids.[1,6-9] In the bulk material at ambient pressure, the hcp structure is always favored over the fcc state in the calculations based on pairwise interactions, even after accounting for three-body terms.[1,9] Zero-point vibrational effects change the situation in favor of the fcc over hcp owing to the coupling between the harmonic modes.[9] Experimentally, the near degeneracy of the fcc and hcp structures is manifested through occasional observation of the latter, but only in small amounts. Examples include bulk Kr and Xe grown well below the freezing temperature,[10] high-purity polycrystalline Ar frozen from the liquid,[11] and Ar clusters produced in supersonic jets.[12] The hcp fraction is associated with non-equilibrium sample growth.[10,12] It is unstable in the bulk samples and can be eliminated by thermal cycling[10] or plastic deformation.[11]

For rare-gas nanoclusters comprising less than N~10^5 atoms, different structures are predicted.[13-15] Their comparative energetics are driven by large differences in the binding energy (up to several percent) owing to the surface contribution. They consist of nearly perfect fcc fragments joined by twin faults, giving rise to particles with five-fold symmetry (for N>13). These are icosahedral for clusters of a few thousands of atoms, and decahedral for larger clusters (Fig. 1). The predictions were confirmed experimentally[16] for N<10^4. Theories also predicted that depending on shapes, sizes and incompleteness of the outermost shells, decahedra, fcc and hcp clusters can alternate over large size intervals and possibly form mixtures of clusters belonging to different symmetries.[9,15,17] For N>10^5 either the hcp clusters may be dominant,[15] or fluctuations could stabilize the fcc structure.[9] Thus, the ground state of the large RGS clusters still remains an important open issue.

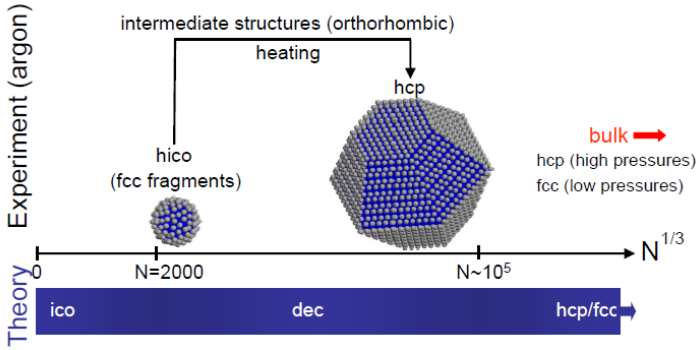

Figure 1 (color online). Theoretically-predicted structures of the classical rare gas solids (bottom), and experimental results for argon (top). *Ico* and *dec* refer to icosahedral and decahedral clusters, respectively. We demonstrate in this work that argon clusters are icosahedral (fcc-like) for small cluster sizes N, and transform to hcp as they grow by fusion with increasing temperature. The hcp structure forms for cluster sizes of N~65000, in good agreement with theoretical predictions.[14,15]

Nanoclusters present an intriguing opportunity to study the RGS structure problem by systematic tests of the predicted dependence of the cluster structure on the cluster size. Confirmation of the expected transformation of the fcc-like clusters into larger hcp particles is especially important because the fcc-to-hcp transition has never been observed in bulk RGS at ambient pressure. Rare-gas nanoclusters can be produced in supersonic jets,[12,18,19] porous media,[20] and by injection of the diluted rare gas into liquid helium.[16,21] Unfortunately, none of the existing experimental techniques has yet allowed the systematic production of the isolated ground-state RGS nanoclusters in the required range of sizes in a controlled environment suitable for structural studies. Importantly, even if the clusters are made, one needs to ensure that the lowest-energy structure is realized. While the fcc-hcp energy difference is tiny, the energy barrier for the fcc-to-hcp transformation is large. This is evidenced, for instance, by the sluggishness of the pressure-induced fcc-to-hcp transformation,[22-25] in which high-energy intermediate structures are proposed to be involved.[3,7] Thus, large RGS clusters grown by a slow aggregation may not exhibit the lowest energy structure. The clusters grown in supersonic jets are often strongly out of equilibrium, and sometimes cannot even be assigned a definite temperature.[26] Enough energy needs to be supplied during the cluster growth for the system to overcome the barriers and realize the ground state. The system should also be given sufficient time to explore the energy landscape, and spatial constraints should be minimized.

In our work, argon nanoclusters are produced by injection of a helium gas jet with ~1% Ar admixture into superfluid helium. This method, known as the impurity-helium gas injection technique,[27] works for rare gases, as well as for many other chemical species (the "impurity"). Separated clusters grow via coalescence of the impurity atoms and their solidification and thermalization in a helium vapor[28]. They are stabilized in liquid helium and remain separated or in minimum contact, arguably protected by formation of strongly-attached "coats" of helium atoms. The nanoclusters form soft, aerogel-like macroscopic (~cm^3) structures with typical average densities between 0.1%-2% of the bulk material

density. For many compositions, including Ar, the clusters can be stable at elevated temperatures outside liquid helium[21,27,29]. With increasing temperature, such "dry" clusters grow, probably by fusion due to the gradual loss of their protective helium coats. The average density also increases, but does not exceed 2-3% of its bulk value. At a certain higher species-dependent temperature, the clusters fuse in an explosion-like process, forming bulk microcrystallites.

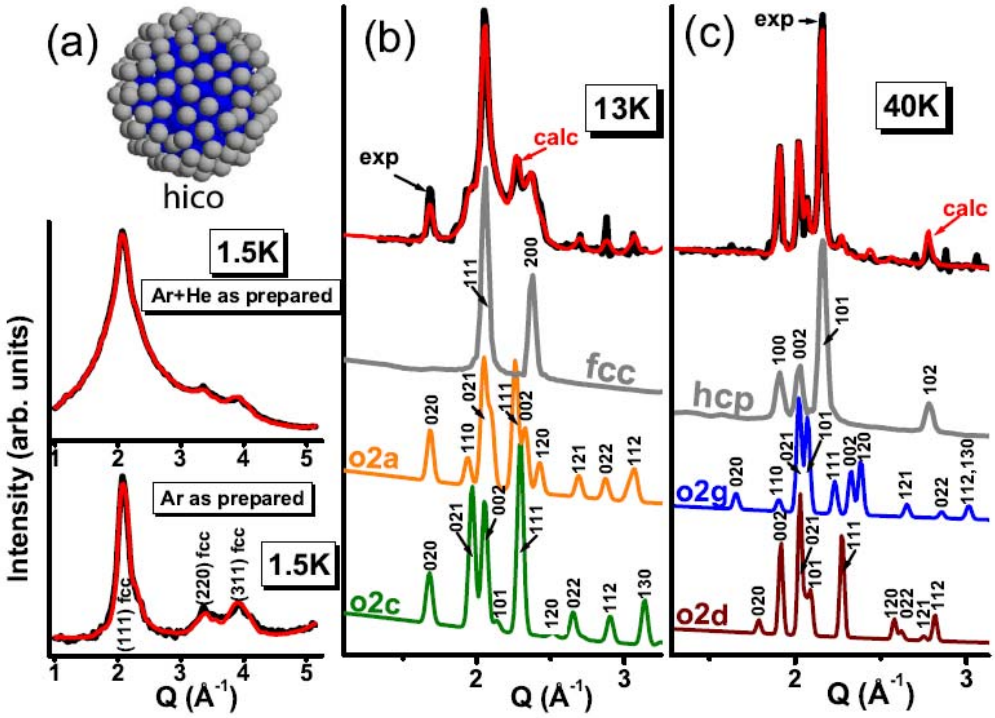

Figure 2 (color). Experimental (black) and calculated (red) x-ray diffraction patterns for Ar nanoclusters. (a) As prepared in liquid helium (middle), and with liquid helium signal subtracted (bottom), for T=1.5 K. The sample consists of icosahedral clusters (top). (b) and (c): On warming to T=13 K and then to T=40 K. The fits (red) are for the mixed fcc-like, hcp (T=40 K only), and the intermediate ($P2_12_12_1$ orthorhombic) structures discussed in the text and given in Table I.[35] The lowest two curves show representative patterns for the orthorhombic intermediate structures accounting for the diffraction peaks originating from neither the fcc nor the hcp structures. The calculated patterns for perfect fcc and hcp clusters (N~3-4×10^4 atoms) are shown in gray. All the peaks are indexed according to the listed crystallographic symmetry. For T=40 K, the scattering pattern is clearly dominated by the signal from the hcp structure.

The structure of the Ar nanoclusters obtained was determined using x-ray diffraction. The experiments were done on beam line X21 at the National synchrotron Light Source, using 12 keV x rays and standard θ-2θ scans. For the data presented here, signals from the empty sample cell were subtracted, and an x-ray polarization correction was made. Argon nanoclusters were made at T=1.5 K using the helium-impurity gas injection technique in a cryostat suitable for x-ray diffraction measurements described in Ref. [21]. The samples were held in a beryllium can with a ~1 cm^3 volume. For experiments at T>4.2 K, liquid helium was evaporated from the sample cell, and the sample was held in a temperature-controlled helium gas flow in low vacuum. On heating above T=40 K, the sample collapsed and was blown out of the sample cell. The results of these measurements are shown in Fig. 2. The powder x-ray diffraction patterns were fitted using the reliability factor (R-factor) minimization, as described in Refs. [16,20]. The R-factor was defined as $R=\Sigma|I_{exp}-I_{calc}|/\Sigma|I_{exp}+I_{calc}|$, where I_{exp} and I_{calc} are the experimental and calculated x-ray intensity, respectively. The analysis of the T=1.5 K data was reported previously.[16] The clusters are icosahedral particles covered over their entire (111) faces by one layer of atoms in hcp-like positions. They are called hexagonal icosahedra (hico), or anti-Mackay clusters.[30] The average particle size is ~3500 atoms. The clusters are comprised of fcc fragments, and therefore the diffraction patterns exhibit the qualitative features typical of a bulk crystal, i.e. the fcc reflections (111), (220), and (311). The relative intensities of these reflections differ from those typical of fcc, reflecting the icosahedral structure of the clusters. As the temperature is increased to 13 K, the Bragg peaks sharpen, reflecting the cluster growth, and additional peaks appear. Some of them cannot be ascribed to either the fcc or the hcp structure, implying presence of intermediate structures. For T=40 K, however, the diffraction pattern is typical of the hcp structure, with only small differences. These results clearly show that as the clusters grow, the majority of them transform from the particles composed of fcc fragments to the hcp structure. These conclusions are summarized schematically in Fig. 1.

For a quantitative analysis of these results, a model for the intermediate structure(s) is needed. Two theoretical schemes of the fcc-to-hcp transformation are available in the literature, one based on monoclinic (m), and the other on orthorhombic (o1) intermediate structures, see Fig 3. In the monoclinic mechanism,[3,7] a basal plane of the initial fcc lattice transforms into the basal plane of the final hcp structure, and the angle α (see Fig. 3) changes from 70.5° to 90°. In the o1 scheme,[3,7] the lattice parameters *a*, *b*, *c* gradually change from 5.31 A (the fcc lattice constant a_{fcc} at 5 K) to the values $a=a_{hcp}$, $b=\sqrt{3}a_{hcp}$, $c=c_{hcp}$ appropriate for the hcp lattice in the orthorhombic representation. In the both cases, every second *ab* plane shifts in the *b* direction by ~*b*/6. Using these models, we calculated the trial diffraction patterns varying the parameters *a*, *b*, *c*, α in the full range. More than 1000 trial sets containing combinations of these patterns were considered, and none of them fitted the experimental results acceptably. Thus, a new transformation mechanism was sought. In this, a small triclinic distortion (5-10%) was applied to the above trial structures. Several of the distorted structures produced a noticeably improved fit to the data. These structures were then relaxed using the steepest descent method applying the well-known Aziz potential for Ar,[31] as described in Refs. [32,33]. The relaxed structures suggested that the transformation could proceed via a previously unknown orthorhombic transition mechanism, which we denote orthorhombic-2 (o2). The space group of the o2 structure is $P2_12_12_1$; its elementary cell is shown in Fig. 3. There are 4 atoms in this cell in the positions *x,z,y; ½-x,½+z,-y; ½+x,-z,½-y; -x,½-z,½+y* (*z* and *y* exchanged to keep the sequence *b>c>a* common for the structures discussed here). For the initial fcc structure, *x*=-1/4, *z*=-1/8, *y*=0, and $a=a_{fcc}/\sqrt{2}$, $b=\sqrt{2}a_{fcc}$, $c=a_{fcc}$. (Note that this is not a conventional fcc unit cell. The axes directions, as well as the origin, are different, as shown in Fig 3.) As the fcc transforms to the hcp structure, the parameters continuously change to *x*=0, *z*=-1/12, *y*=0, and $a=a_{hcp}$, $b=\sqrt{3}a_{hcp}$, $c=c_{hcp}$. As in the o1 scheme, the orthorhombic axes transform into the corresponding axes of the hcp structure in the orthorhombic representation, see Fig. 3.

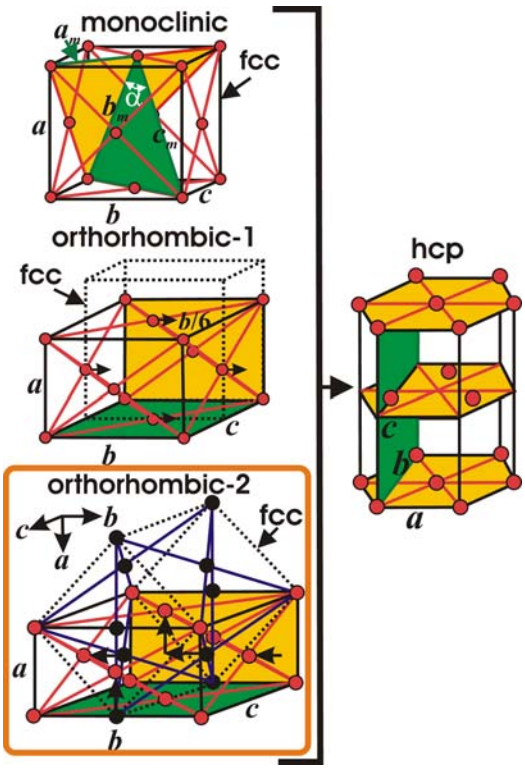

Figure 3 (color online). Model transformation schemes from the fcc to the hcp structure. The basal triangular close-packed planes are shown in yellow (light gray), and the *bc* planes in green (dark gray). As the fcc structure transforms into the hcp, the atoms shift as shown with black arrows (see the text for details). In the monoclinic scheme, the angle α changes from 70.5° to 90°, and the lattice parameters a_m, b_m, c_m become the *a, b, c* of the hcp lattice in the orthorhombic representation (shown at right). In the orthorhombic schemes, the unit cell axes also transform into the orthorhombic *a, b, c* of the hcp lattice. Only the new orthorhombic scheme proposed in this work, orthorhombic-2, successfully describes the experimental diffraction patterns shown in Figure 2.

The o2 intermediate structure reproduces all the extra Bragg peaks in our data. The experimental diffraction patterns are very well fit assuming that only the o2 clusters, fcc material with a few deformation-type stacking faults (observed previously in RGS clusters, see Ref. [16]), and the hcp particles (*T*=40 K only) are present, see Fig. 2. The initial fit was obtained using the o2 model for *T*=13 K, and the hcp structure for *T*=40 K. Contributions due to additional structures were then added to the calculated diffraction patterns, until satisfactory agreement with the data was attained. For clusters containing less than 40000 atoms, the diffractograms were calculated using the Debye equation[34]. For the larger clusters, the Bragg peak intensities were calculated using the standard formula for an infinite

crystal, with the peaks broadened due to the finite particle size effect. Gaussian broadening and the Scherrer equation[34] were used in the latter case. For the fits shown in Fig. 2, the *R*-factor was *R*=0.039 for *T*=13 K, and *R*=0.063 for *T*=40 K. The structure types and the average sizes of the clusters derived from the x-ray data are shown in Figure 4. Supplementary Table I gives the numerical parameters and relative contributions of these structures.[35] The appearance of multiple structures is natural for our inhomogeneous samples, which may exhibit material at different stages of the fcc-to-hcp transformation due to the differences in the local energy release during cluster fusion. We note that no structures with unphysical parameters were allowed. While the energies of nearly all the o2 clusters (calculated using the Aziz potential[31]) approach the melting energy, they do not exceed it. This is appropriate for this system, which contains much surface energy that is released locally when the clusters fuse. The observed dispersion of the unit cell volumes (5-10%) in Table I[35] is consistent with the range of compressions typical of the icosahedral clusters. While our results do not exclude some other unknown fcc-to-hcp transformation mechanism, the o2 scheme provides a simple and satisfactory description of the experimental data. A detailed theoretical study of this new mechanism would certainly be of interest, especially in the context of the well-known pressure-induced fcc-to-hcp transition in RGS.

Fig. 4 summarizes the results of this analysis. Initially, icosahedral clusters containing ~3500 atoms are created. The clusters comprise fcc fragments connected via twin faults. On warming from *T*=1.5 K to 13 K, the clusters grow and the system contains both the fcc particles with defects and the intermediate structures, presumably orthorhombic. On further heating to *T*=40 K, the majority of the clusters (~60%) transform to the hcp structure. The average particle size is ~65000 atoms at this temperature. These results do not depend on the specific model used for the intermediate structures.

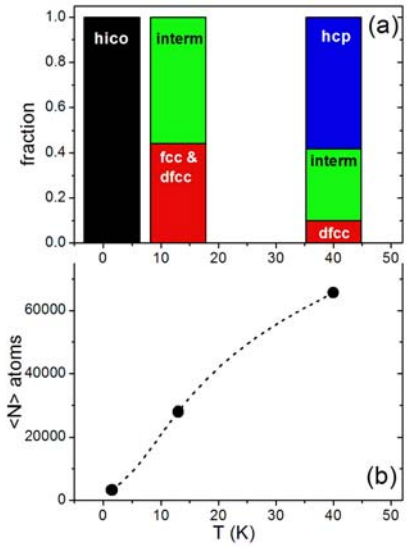

Figure 4 (color online). Volume fractions of the cluster structures (a) and average cluster sizes (b) at different temperatures, derived from the x-ray data. Icosahedral (hico) fcc-like clusters of average size N~3500 atoms are created at T=1.5 K. With increasing temperature, they fuse and grow. For T=13 K, a mixture of the fcc particles (some with defects, dfcc), and the orthorhombic intermediate (interm) structures is observed. For T=40 K, the clusters grow to N~65000 atoms on average, and the majority of the sample consists of hcp particles. Dashed line in (b) is a guide to the eye.

The main result of our work is observation of transformation of the essentially fcc particles into the hcp clusters as they grow from ~3500 to ~65000 atoms at low pressure (essentially, in vacuum). This is consistent with the theoretical predictions of Refs. [14,15], and does not support the studies predicting the fcc strucure[9,13] While the fcc-hcp phase coexistence was reported in Kr and Xe when they crystallize below $0.65T_f$ (T_f is the freezing temperature) at ambient pressure,[10] no low-pressure fcc-to-hcp transition has been previously observed in any RGS. In our samples, the cluster growth occurs via particle fusion on warming. A large amount of energy is released in the process–a cluster of 10^4 atoms stores about a quarter of its melting energy on its surface. The low density of this system prevents easy dissipation of this energy, and it allows the majority of the fusing particles to eventually overcome the fcc-hcp energy barrier. A large energy landscape is explored in this process, and high-energy intermediate structures can form, as observed in our measurements. Cluster growth is unimpeded in

most directions due to the low particle density. It appears probable that the conditions necessary to achieve the ground state are realized in our experiments: sufficient energy is available during the cluster growth, and no spatial constraints are present. The crystallization kinetics, energy input, and spatial constraints therefore are of the key importance for the outcome of the RGS growth. Our results show that the extant theory[14,15] correctly predicts the structures of the RGS clusters comprising up to ~10^5 atoms. The surface atomic fraction in these clusters is still significant, and studies of larger clusters are needed to understand the structure of the bulk RGS. We believe that such studies hold significant potential for understanding the various factors affecting the RGS growth, and for the eventual solution of the RGS structure problem.

The authors are grateful to C.S. Nelson for help with x-ray experiments. This work was supported by the NSF grant No. DMR-1209255, by the Norman Hackerman Advanced Research Program under grant No. 010366-0137-2009, and by CRDF grant No. RUP1-7025-CG-11.

References

1. J.A. Venables, in *Rare Gas Solids*, edited by M.L. Klein, and J.A. Venables, (Academic Press, London, 1976).
2. B.W. van de Waal, Phys. Rev. Lett. **67**, 3263 (1991).
3. E. Kim and M. Nicol, Phys. Rev. Lett. **96**, 035504 (2006).
4. I. Kwon, L.A. Collins, J.D. Kress, N. Troullier, Phys. Rev. B **52**, 15165 (1995).
5. J.K. Dewhurst, R. Ahuja, S. Li, B. Johansson, Phys. Rev. Lett. **88**, 075504 (2002).
6. Yu. Freiman, A.F. Goncharov, S.M. Tretyak, A. Grechnev, J.S. Tse, D. Errandonea, H.-k. Mao, R. Hemley, Phys. Rev. B **78**, 014301 (2008).
7. N.V. Krainyukova, Low Temp. Phys. **37**, 435 (2011).
8. Yu. Freiman and S.M. Tretyak, Low Temp. Phys. **33**, 545 (2007).
9. P. Schwerdtfeger, N. Gaston, R.P. Krawczyk, R. Tonner, G.E. Moyano, Phys. Rev. B **73**, 064112 (2006).
10. Y. Sonnenblick, Z.H. Kalman, I.T. Steinberger, J. Cryst. Growth **58**, 143 (1982).
11. L. Meyer, C.S. Barrett, P. Haasen, J. Chem. Phys. **40**, 2744 (1964).
12. A.G. Danil'chenko, S.I. Kovalenko, V.N. Samovarov, Low Temp. Phys. **34**, 966 (2008).
13. B. Raoult, J. Farges, M.-F. de Feraudy, G. Torchet, Philos. Mag. B **60**, 881 (1989).
14. N.V. Krainyukova, Thin Solid Films **515**, 1658 (2006).
15. N.V. Krainyukova, Eur. Phys. J. D **43**, 45 (2007).
16. V. Kiryukhin, E.P. Bernard, V.V. Khmelenko, R.E. Boltnev, N.V. Krainyukova, D.M. Lee, Phys. Rev. Lett. **98**, 195506 (2007).
17. T.P. Martin, Phys. Rep. **273**, 199 (1996).
18. J. Farges, M.F. de Feraudy, B. Raoult, G. Torchet, J. Chem. Phys. **78**, 5067 (1983).

19. O.G. Danylchenko, S.I. Kovalenko, V.N. Samovarov, Low Temp. Phys. **30**, 166 (2004).
20. N.V. Krainyukova and B.W. van de Waal, Thin Solid Films **459**, 169 (2004).
21. V. Kiryukhin, B. Keimer, R.E. Boltnev, V.V. Khmelenko, E.B. Gordon, Phys. Rev. Lett. **79**, 1774 (1997).
22. A.P. Jepcoat, H-k. Mao, L.W. Finger, D.E. Cox, R.J. Hemley, C.-S. Zha, Phys. Rev. Lett. **59**, 2670 (1987).
23. H. Cynn, C.S. Yoo, B. Baer, V. Iota-Herbei, A.K. McMahan, M. Nicol, S. Carlson, Phys. Rev. Lett. **86**, 4552 (2001).
24. D. Errandonea, B. Schwager, R. Boehler, M. Ross, Phys. Rev. B **65**, 214110 (2002).
25. D. Errandonea, R. Boehler, S. Japel, M. Mezouar, L.R. Benedetti, Phys. Rev. B **73**, 092106 (2006).
26. C.E. Klots, Nature **327**, 223 (1987).
27. E.B. Gordon, L.P. Mezhov-Deglin, O.F. Pugachev, JETP Lett. **19**, 63 (1974).
28. E.A. Popov, J. Eloranta, J. Ahokas, H. Kunttu, Low Temp. Phys. **29**, 510 (2003).
29. S.I. Kiselev, V.V. Khmelenko, D.M. Lee, V. Kiryukhin, R.E. Boltnev, E.B. Gordon, B. Keimer, Phys. Rev. B **65**, 024517 (2001).
30. J.P.K. Doye, D.J. Wales, R.S. Berry, J. Chem. Phys. **103**, 4234 (1995).
31. R.A. Aziz and M.J. Slaman, Molec. Phys. **58**, 679 (1986).
32. N.V. Krainyukova, J. Low Temp. Phys. **150**, 317 (2008).
33. N. Krainyukova and V. Kraynyukov, J. Phys. CS **150**, 032047 (2009).
34. B. E. Warren, *X-Ray Diffraction* (Addison-Wesley, Reading, MA, 1969).
35. See Supplemental Material at [*URL will be inserted by Publisher*] for Table I.